Pharm Res (2012) 29:2139–2156
DOI 10.1007/s11095-012-0743-3

RESEARCH PAPER

# The Effect of Engineered Mannitol-Lactose Mixture on Dry Powder Inhaler Performance

Waseem Kaialy • Hassan Larhrib • Gary P. Martin • Ali Nokhodchi

Received: 25 October 2011 / Accepted: 19 March 2012 / Published online: 5 April 2012


## ABSTRACT

***Purpose*** To co-crystallise mannitol and lactose with a view to obtaining crystals with more favourable morphological features than either lactose or mannitol alone, suitable for use as carriers in formulations for dry powder inhalers (DPIs) using simultaneous engineering of lactose-mannitol mixtures.

***Methods*** Mannitol and lactose individually and the two sugars with three different ratios were crystallised/co-crystallised using anti-solvent precipitation technique. Obtained crystals were sieved to separate 63–90 $\mu$m size fractions and then characterised by size, shape, density and *in vitro* aerosolisation performance. Solid state of crystallized samples was studied using FT-IR, XRPD and DSC.

***Results*** At unequal ratios of mannitol to lactose, the elongated shape dominated in the crystallisation process. However, lactose exerted an opposite effect to that of mannitol by reducing elongation ratio and increasing the crystals' width and thickness. Crystallised β-lactose showed different anomers compared to commercial lactose (α-lactose monohydrate). Crystallised α-mannitol showed different polymorphic form compared to commercial mannitol (β-mannitol). Crystallised mannitol:lactose showed up to 5 transitions corresponding to α-mannitol, α-lactose monohydrate, β-lactose, 5α-/3β-lactose and 4α-/1β-lactose. *In vitro* deposition assessments showed that crystallised carriers produced more efficient delivery of salbutamol sulphate compared to formulations containing commercial grade carriers.

***Conclusion*** The simultaneous crystallization of lactose-mannitol can be used as a new approach to improve the performance of DPI formulations.

**KEY WORDS** fine carrier · *in vitro* aerosolisation · mannitol: lactose ratio · salbutamol sulphate · shape · size · solid state · roughness

## INTRODUCTION

The respiratory tract provides an attractive delivery route due to a number of potential advantages that it confers, such as the avoidance of the harsh conditions of the gastrointestinal tract, the provision of fast drug action or absorption, and the ability to target specific lung cells. Indeed, systems designed for both local and systemic action can be administered via the pulmonary portal. In local systems, a number of patient factors pose unique challenges to effective drug delivery including: the pattern of inspiratory airflow, the physiology and anatomy of the respiratory tract and the proficiency of the patient in handling the aerosolization device. In addition to obtain successful local pulmonary delivery, it is crucial to consider several formulation-related factors including: selection of the specific drug, identification of the receptor locations, the design of the device and the nature of the incorporated formulation. Dry powder inhalers (DPIs) are one type of delivery device with the capacity to deliver respirable drugs to the lungs and have potential advantages which include the containment of propellant-

W. Kaialy · A. Nokhodchi (✉)
Chemistry and Drug Delivery Group, Medway School of Pharmacy, University of Kent
ME4 4TB, Kent, UK
e-mail: a.nokhodchi@kent.ac.uk

W. Kaialy
Pharmaceutics and Pharmaceutical Technology Department
University of Damascus
Damascus 30621, Syria
e-mail: kaialy_4uu@yahoo.com

H. Larhrib
Faculty of Applied Sciences, University of Huddersfield
Queensgate, Huddersfield, West Yorkshire HD1 3DH, UK

G. P. Martin
King's College London, Institute of Pharmaceutical Science
Franklin-Wilkins Building, 150 Stamford Street
London SE1 9NH, UK

free formulations and patient-initiated actuation. Most powdered formulations intended for aerosolization from DPIs comprise a blend of 1–5 μm drug with a sugar carrier (approximately 100 μm diameter). However, despite their current widespread use as a delivery system; drug-carrier formulations performance is dependent on several factors. For example, the inhalable fraction obtained from a DPI is dependent on inhaler device design (1), patient inhalation effort (2) and powder formulation properties (3). Generally the amounts of drug delivered to the lower airway regions from the current DPIs are still low (often ≤25% of theoretical dose), indicative of low delivery efficiency (4). In order to enhance DPI performance, several attempts have been made such as using engineered drug (5) and carrier (6) particles. Nevertheless, the effects of carrier physical properties on DPI aerosolization efficiency are equivocal. For example, the fine particle fraction (FPF) of drug generated by aerosolization of the powder has been reported to be dependent on the drug-carrier cohesive-adhesive balance ratio, regardless of other carrier physicochemical properties such as size, shape, rugosity, and flowability (7). Generally, larger carrier particles generated poorer DPI aerosolization performance (8). However, other studies have indicated that poor aerosolization performance is a not a property inherent to larger size of carrier particles (9,10). Also, it has been suggested that it is the presence of fine carrier particles and not the carrier particle size that directly affects DPI performance (11). Two major mechanisms are believed to control drug particle detachment from carrier particles during inhalation which are detachment by the flow stream (fluid forces) (flow detachment) and detachment by impaction (mechanical forces) (mechanical detachment) (12). Detachment by flow is facilitated for flat, smooth surface carrier particles and large drug particles, whereas detachment by mechanical forces is facilitated for large drug and carrier particles (9). It was shown that the aerodynamic performance of carrier particles is dependent not only on their physical properties (e.g. size and morphology), but also on the inhaler device design (12). DPI formulations containing carriers with different size distributions generated similar emitted dose and recovery of drug upon inhalation (13). DPI performance was reportedly enhanced by employing carrier particles with higher elongation ratio (14,15). However, other studies showed that engineered carrier particles produced better DPI performance despite their lower elongation ratio in comparison to control (3,16). Several reports have confirmed that fine carrier particles can enhance DPI performance, but the estimated optimal concentration of fine carrier particles to maximize FPF apparently varies from 5% (17), 9–10% (18), 20% (19), 37.5% (20) to 50% (21). Also, carrier specific surface area has been correlated both positively (14) and negatively (22) with FPF of drug. Better aerosolization performance was observed when the carrier powder tap density was lower (14), whilst formulations with good flow properties (23) and poor flow properties (14) produced increased FPF. A higher FPF was obtained when using DPI blends containing particles with either increased surface rugosity (3) or increased surface smoothness (6).

These conflicting results could, in part, be attributed to inter-dependence of different carrier physical properties on each other. For example, both carrier surface roughness (24) and polymorphic form (25) were reported to dominate over carrier particle size while fine carrier particle content can dominate over both carrier size and surface roughness in terms of their influence on DPI performance (26). Accordingly, there are no definite conclusions showing the optimum morphology for carrier particles in DPI systems. Mannitol presents several advantages compared to lactose and other sugar alcohols, since it does not contain a reducing functional group and does not contain or made of animal material. Lactose and mannitol are expected to crystallise with considerably different morphologies as reported in our previous work (3,14). Thus, co-crystallisation of mannitol-lactose at different ratios of mannitol to lactose might generate suitable crystals with the desired morphological features with applicability for use as a carrier in DPIs. In addition, mannitol or lactose may act as an impurity in the crystallisation medium, modifying the co-nucleation or co-growth, of each sugar leading to particles with different size and shape properties. Additives such as surfactants and polymers are commonly used to inhibit crystal growth. However, there is concern with the use of such additives with respect to their safety for delivery to the lungs. Any adsorbed material on the surface of the formed crystals requires removal using an organic solvent and in addition to possible toxicological considerations, care is required to avoid crystal morphological changes. The primary aim of this work was to crystallise mannitol and lactose separately and co-crystallise mannitol:lactose using different ratios of mannitol to lactose (15:05, 10:10, 05:15*w*/*w*). The objective was then to employ this range of carriers, alongside commercial lactose (CL), commercial mannitol (CM) to prepare DPI formulations

to investigate the deposition profiles of salbutamol sulphate *in vitro*.

## MATERIALS AND METHODS

### Materials

D-mannitol and α-Lactose-monohydrate (Pharmatose, 100 M) were obtained from Roquett, France and DMV International, the Netherlands respectively. Micronized salbutamol sulphate was obtained from LB Bohle, Germany. Acetone was purchased from Roquett, France.

### Preparation of Different Carrier Powders

Different batches of crystallised powders containing mannitol:lactose in different ratios were prepared using anti-solvent precipitation technique. First, physical mixtures were prepared by mixing different ratios of commercial mannitol (CM):commercial lactose (CL) (20:0, 15:05, 10:10, 05:15, 0:20) in Turbula mixer for 15 min/100 rpm. After blending, each mannitol:lactose powder (20 g) was dissolved in distilled water (solution final volume is 100 mL)under stirring (200 rpm) and heating (35°C) to produce 20% (w/v) different sets of saturated solutions maintained at 35°C. Both mannitol and lactose are poorly soluble in acetone which is miscible with the lactose:mannitol solvent (water), and therefore, acetone was selected as anti-solvent to prepare crystallised mannitol:lactose products. This anti-solvent was raised to 30±1°C and maintained at this temperature throughout the co-solvent induced precipitation process for all samples. A 20 mL portion of each mannitol:lactose saturated solution was added using a syringe to a constant volume of acetone (100 mL) at a constant rate of 2.5 mL/min, whilst the mixture was stirred (300 rpm). After adding the total volume of mannitol:lactose, the resultant suspensions were removed from heating and left uncovered in a 250 mL beaker to cool to room temperature (ca. 22°C) and maintained at this temperature for 30 min. The crystals were collected by filtration (under vacuum) through a Whatman cellulose filter paper (pore size <0.45 μm) fitted into a filtration unit. The crystals were spread on a glass Petri dish and left to dry in a ventilated oven (LTE Scientific Ltd, UK) for 24 h at 60°C. The dried crystals were transferred to glass vials, which were sealed and the batches stored under ambient laboratory conditions (21±2°C, 50±5% RH) until required for further investigation. Each batch was prepared in duplicate under identical conditions at different times with a view to providing some assessment of the reproducibility of the process.

### Selecting of Carrier Particle Size Fraction

In order to minimize the effect of carrier particle size on subsequent tests, similar sieved size fractions (63-90 μm) were used for all carrier samples. This was achieved by mechanical sieving for 15 min as described in details elsewhere (14). All analyses described below were performed on sieved fractions.

### Particle Size Measurements

Particle size analysis was conducted using a Sympatec (Clausthal-Zellerfeld, Germany) laser diffraction particle size analyzer operated according to the experimental procedure described previously (6).

### True Density Measurements

The true density of all carrier samples was determined using an ultrapycnometer 1000 (Quantachrom, USA) under helium gas. The input gas pressure was 19 psi and the equilibrium time was 1 min.

### Particle Image Analysis

Quantitative optical image analysis was performed using a computerized morphometric analyzing system (Leica Q Win Standard Analyzing Software and Leica DMLA Microscope; Leica Microsystems Wetzlar GmbH, Wetzlar, Germany). For each sample, a small amount of powder (~20 mg) was homogenously sprinkled onto a microscope slide and a minimum 3000 particles were detected and measured. Several morphology descriptors were employed to quantify the morphology of carrier particles including elongation ratio ($R_{elongation}$, Eq. 1:a fundamental first order form descriptor), shape factor ($F_{shape}$, Eq. 2) and surface factor ($F_{surface}$, Eq. 3:second order form descriptors reflecting variations in particle shape regularity and surface roughness), simplified shape factor ($e_R$, Eq. 4:a morphology descriptor which takes into account, in combination, variation in surface roughness and circularity), angularity (Eq. 5:a second order shape descriptor which is complimentary to $F_{shape}$ and independent of both particle surface texture and $R_{elongation}$), compactness (Eq. 6:a measure of circular particle cross sectional circularity), and roughness (Eq. 7:a

third order shape property which is independent of both first order properties and second order parameters):

$$R_{elongation} = \frac{Length}{Width} \quad (1)$$

$$F_{shape} = 4 \times \pi \times \frac{Area}{perimeter^2} \quad (2)$$

$$F_{surface} = F_{shape} \times \frac{\left(1 + R_{elongation}\right)^2}{\pi \times R_{elongation}} \quad (3)$$

$$e_R = \frac{ConvxPerim}{Perimeter} - \sqrt{1 - \left(\frac{breadth}{length}\right)^2} \quad (4)$$

$$Angularity = \frac{Perimeter_{convex}}{\sqrt{\frac{1+AR^2}{2\times AR}}\,Perimeter_{circle}}^2 \quad (5)$$

$$Compactness = \frac{Perimeter^2}{Area} \quad (6)$$

$$Roughness = \frac{Perimeter}{ConvxPerim} \quad (7)$$

A circle or ellipse will have an angularity of 1 whereas particles that are more angular in shape will have a higher value. Also, a perfect circle has a compactness value of $4\pi$ whereas a line will have compactness of infinity.

## Scanning Electron Microscope (SEM)

Scanning electron micrographs of salbutamol sulphate (SS), carriers, and SS-carrier formulations were obtained using a scanning electron microscope (Philips XL 20, Eindhoven, Netherlands) operated at 15 kV. The specimens were mounted on a metal stub with double-sided adhesive tape and coated under vacuum with gold in an argon atmosphere prior to observation.

## Fourier Transform Infrared Spectroscopy (FT-IR)

All samples were assayed using a SPECTRUM-ONE FT-IR (PerkinElmer, Massachusetts, USA) spectrometer, using a scanning range of 450–4000 $cm^{-1}$with a 1 $cm^{-1}$ resolution at room temperature. Each sample (several milligrams) was placed on the middle of the sample stage and force was applied by the top of the arm of the sample stage. A Force gauge was applied ($50 \pm 2$ arbitrary units of the device's pressure meter) to make the necessary contact to yield a characteristic spectrum. After obtaining sharp peaks with reasonable intensities, the spectra acquired were the results of averaging four scans.

## Differential Scanning Calorimetry (DSC)

A DSC7 (Mettler Toledo, Switzerland) was employed with nitrogen as the purge gas and the latter was adjusted to a flow rate of 50 mL $min^{-1}$ through the DSC cell. Aluminium non-hermetic DSC pans were used through the study. The mass of each empty sample pan was matched with the mass of the empty reference pan to $\pm 0.1$ mg. The instrument was calibrated using an indium and zinc standards; approximately 4–5 mg of sample was used for each run. After sealing, the pans were placed in the DSC furnace which had been pre-equilibrated at 25°C. Before each measurement, the sample was allowed to equilibrate for 5 min at 25°C and was then heated to 300°C at a heating rate of 10°C $min^{-1}$. Each sample was analysed in triplicate.

## X-Ray Powder Diffraction (XRPD)

A Siemens diffractometer (Siemens, D5000, Germany) was used with the cross-section of samples being exposed to X-ray radiations (Cu Kα) which had a wavelength of 1.5406 Å. Samples were placed into a stainless steel holder and the surface of powder was levelled manually for analysis. The sample was scanned between 5 and 50 of 2θ with a step size and time of 0.019° and 32.5 s, respectively.

## Preparation of SS-Carrier Formulations

Salbutamol sulphate powder (16) was mixed separately with each carrier powder (3 g) in a ratio of 1:67.5 (*w*/*w*), in cylindrical aluminium container (6.5×8 cm). This blending was carried out using a Turbula® mixer (Willy A. Bachofen AG, Maschinen fabrik, Basel, Switzerland) at standard mixing conditions (100 rpm speed and 30 min mixing time) for preparation of all formulations. A total of 7 formulations with CM, CL, and 5 different crystallised mannitol:lactose carrier powders were prepared using identical mixing conditions.

## Homogeneity Test

After blending, the homogeneity of SS content in each of the formulation was examined by taking a minimum of five randomly selected samples ($33 \pm 1.5$ mg, corresponding to a unit SS dose: $481 \pm 22$ μg) from different sites within the formulation mixture (this weight of powder was then equalized to the filling weight in each capsule). Each sample was

subsequently dissolved in 100 mL of distilled water and assayed for SS content using the HPLC method described elsewhere (14). The homogeneity of powder formulations was assessed using the coefficient of variation (% CV).

### Drug-Carrier Adhesion Assessments

Air depression sieving was employed to assess SS-carrier adhesion forces. A 45 μm sieve (Retsch®GmbhTest Sieve, Germany) was employed and the air jet sieving machine (Copley Scientific, Nottingham, UK) was operated at a gas volume flow that generated a negative pressure of 40 hPa (4 KPa). No effective loss of particles was detected from any of the 63–90 μm carrier samples after 3 min of air jet sieving, indicating the suitability of 45 μm sieve to assess SS-carrier adhesion. An accurately weight quantity of 1 g of each formulation was placed on top of the 45 μm sieve and four samples (33±1.5 mg) were removed from different areas of the formulation after different functional sieving times. The SS content in each formulation sample was quantified using HPLC (14) and expressed as a percentage of the average SS content determined initially in each blend before sieving. Assuming that particle adhesion force correlates with particle detachment force, should less amounts of SS remain on top of 45 μm sieve then this is indicative of weaker drug-carrier adhesion. Adhesion assessments were conducted in an air-conditioned laboratory (21°C and 50% RH).

### *In Vitro* Deposition Study Using Multi Stage Liquid Impinger (MSLI)

Each formulation was filled manually in a hard gelatin capsules (size 3), such that each capsule contained 33± 1.5 mg powder. Following filling, capsules were stored in sealed glass vials at ambient conditions (21±2°C, 50 ±2% RH) for at least 24 h prior to investigation and experiments were carried out within 7 days of filling. Deposition profiles of different blends were assessed *in vitro* using an Aerolizer® inhaler device with MSLI equipped with a USP induction port (IP, Copley Scientific, Nottingham, UK) at flow rate of 92 L/min corresponding to a pressure drop of 4 kPa across the device. Each deposition experiment was carried out as detailed elsewhere (14) and involved the actuation of ten capsules per experiment, each experiment being repeated a further two times (i.e. $n=3$) in an air-conditioned laboratory (21±2°C, 50±2% RH). Several parameters were employed to characterize deposition profiles for all formulations under investigation including: recovered dose (RD), emitted dose (ED), impaction loss (IL), mass median aerodynamic diameter (MMAD), geometric standard deviation (GSD), fine particle dose ($FPD_{\leq 5\mu m}$), fine particle fraction ($FPF_{\leq 5\mu m}$, expressed as a percentage of RD), dispersibility (DS) and effective inhalation index (EI) (these terms are defined elsewhere (15,27)). In order to calculate the experimental the mass median aerodynamic diameter (MMAD), the cumulative percentage of drug mass less than the stated aerodynamic diameter of MSLI stages from 1 to 4 was calculated and plotted as a log probability function of the effective cut-off diameter taking cumulative amounts less than MSLI stage 1 as 100%. MMAD is the particle size at which the linear plot crossed the 50% mark (as the 50th percentile of the aerodynamic particle size distribution by mass). The same plot was used to calculate the geometric standard deviation as the square root of the ratio of particle size at the 84.13th percentile to the 15.87th percentile.

### Statistical Analysis

One-way analysis of variance (ANOVA), correlation, and regression analysis were applied, where appropriate, to compare results in this study. A p value less than 0.05 was taken as being indicative of significant difference.

## RESULTS AND DISCUSSION

### Micromeritic Properties

Table I summarises the data obtained for the % yield, volume mean diameter (VMD), concentration of fine particle carrier (FPC), span, and true density ($D_{true}$) for each carrier product. Differently isolated carriers contained particles with different size and size distribution (Fig. 1, Table I) although each batch had been subjected to a similar sieving procedure. For example, the VMD of crystallised carriers was significantly smaller ($p<0.05$) than those of commercial carriers, except for M:L (15:05) which had a VMD which was the same ($p>0.05$) as CL. Crystallised carriers demonstrated significantly higher span values (calculated as: $X_{90\%}-X_{10\%}/X_{50\%}$) ($p<0.05$) than those of the commercial carriers (Table I, Fig. 1), which indicated broader (more heterogonous) size distributions. Such wider size distribution can be ascribed to secondary nucleation and heterogeneous crystal growth resulting from random energy fluctuations within the solution induced by mechanical stirring during crystallisation. Crystallised carriers contained higher concentrations of fine particles less than 5 μm ($FPC_{<5\mu m}$) or less than 10 μm ($FPC_{<10\mu m}$) than the commercial grade carriers, which had no determinable fines (Table I). The relative absence of fines in the latter samples accounts for the lower span values being recorded for these carriers. The fines contained in the crystallised batches refer to intrinsic (non-added) fine carrier particles which adhered to the surfaces of the larger carrier particle with sufficient force such that they were not removed by sieving. Particle size obtained by

**Table I** % Yield, Volume Mean Diameter (VMD), Volume Specific Surface Area ($SSA_v$), Fine Particle Carrier Content ($FPC_{<5\mu m}$, $FPC_{<10.5\mu m}$), Span, and True Density ($D_{true}$) for Commercial Mannitol (CM), Commercial Lactose (CL), and Different Crystallised Mannitol:lactose (M:L) (20:0, 15:05, 10:10, 05:15, 0:20) Products (mean ± SE, $n \geq 5$)

| | CM | CL | M:L (20:0) | M:L (15:05) | M:L (10:10) | M:L (05:15) | M:L (0:20) |
|---|---|---|---|---|---|---|---|
| Yield (%) | .... | .... | 85.2 | 87.0 | 82.3 | 83.3 | 78.4 |
| VMD (μm) | 108.1 ± 0.5 | 91.1 ± 0.2 | 62.3 ± 2.0 | 90.6 ± 2.7 | 73.8 ± 0.6 | 45.8 ± 2.2 | 78.4 ± 1.3 |
| $SSA_v$ ($m^2/cm^3$) | 0.06 ± 0.00 | 0.07 ± 0.00 | 0.43 ± 0.03 | 0.18 ± 0.02 | 0.38 ± 0.01 | 0.39 ± 0.02 | 0.19 ± 0.01 |
| $FPC_{<5\mu m}$ (%) | 0.0 ± 0.0 | 0.0 ± 0.0 | 8.2 ± 0.8 | 2.5 ± 0.5 | 7.3 ± 0.4 | 4.8 ± 0.4 | 2.0 ± 0.3 |
| $FPC_{<10.5\mu m}$ (%) | 0.0 ± 0.0 | 0.0 ± 0.0 | 15.0 ± 1.4 | 3.9 ± 0.7 | 11.2 ± 0.6 | 9.4 ± 0.8 | 4.2 ± 0.6 |
| Span | 0.77 ± 0.01 | 0.80 ± 0.00 | 1.69 ± 0.07 | 0.95 ± 0.06 | 1.42 ± 0.02 | 1.64 ± 0.10 | 1.03 ± 0.06 |
| $D_{true}$ ($g/cm^3$) | 1.52 ± 0.00 | 1.57 ± 0.01 | 1.49 ± 0.00 | 1.49 ± 0.00 | 1.51 ± 0.00 | 1.51 ± 0.01 | 1.53 ± 0.00 |

sieving represents the minimum square aperture through which the particle can pass and despite all carriers being subjected to the same sieving procedure, they may not all have the same strength to resilience to abrasion which may occur during mechanical processing. The crystallised mannitol M:L (20:0) proved to contain the most elongated and the thinnest of all particles (needle-like) (Fig. 4), resulting in the most brittle particles and therefore creating more fines due to particle-particle and particle-sieve wall collision (Table I).

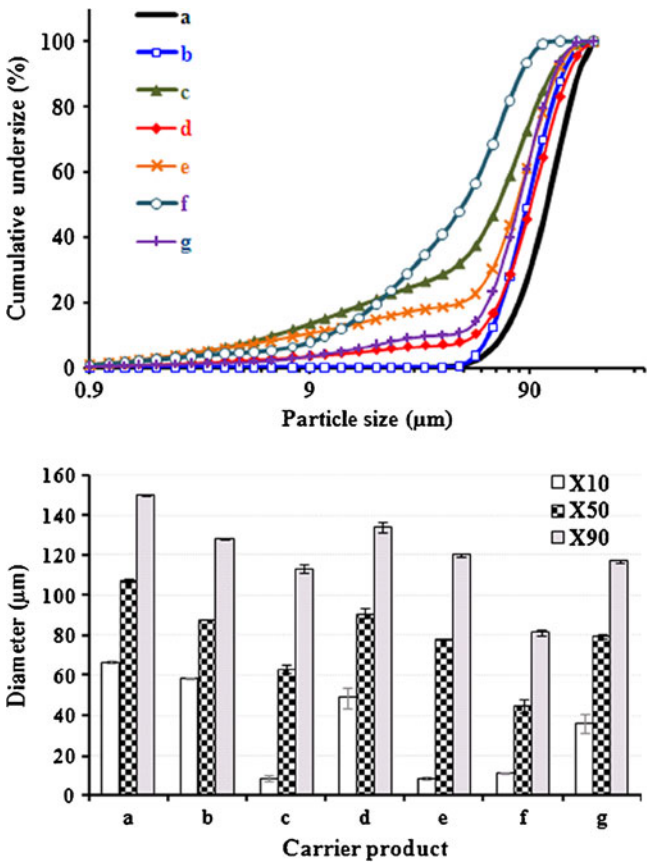


**Fig. 1** Cumulative (% undersize) particle size distribution, 10th, 50th (median), and 90th percentile of volume distribution ($X_{10}$, $X_{50}$, $X_{90}$)for commercial mannitol (**a**) (solid line), commercial lactose (**b**) (□), and different powders crystallised from mannitol (M):lactose (L) mixture combinations comprising M:L 20:0 (**c**) (▲), 15:05 (**d**) (♦), 10:10 (**e**) (x), 05:15 (**f**)(○), 0:20 (**g**)(+)powders(mean ± SE).

The volume specific surface area ($SSA_v$) was considerably higher for all the crystallised carrier particles compared to both commercial carriers (Table I). Interestingly, linear relationships were established between carrier $SSA_v$, span ($r^2$=0.965), $FPC_{<5\mu m}$ ($r^2$=0.928) and $FPC_{<10.5\mu m}$ ($r^2$=0.961) (Fig. 2) indicating higher surface area for carrier samples with wider size distribution and higher fines content. True density ($D_{true}$) measurements indicated that CL has slightly higher $D_{true}$ than CM (Table I). For crystallised carrier particles, the higher the lactose concentration in mannitol: lactose carrier the higher the true density (linear, $r^2$=0.9244, figure not shown) (Table I). Variations in true density could be attributed to differences between different carrier particles in terms of size (Fig. 1, Table I) and crystalline nature (as shown later).

## Image Microscopy Particle Shape Analysis

Individual particle shape descriptors provide different assessments of the variation in particle shape. Figure 3a indicates that both angularity and compactness varied across the range of different carrier particles in the order: CL>CM>crystallised carriers, demonstrating that crystallised carrier crystals are less angular than both CM and CL. Crystallised carrier crystals exhibit higher $F_{shape}$, higher $F_{surface}$, higher $e_R$, and smaller roughness values than commercial carrier particles (Fig. 3b), indicating their relatively more regular shape and smoother surface texture.

Except for carrier particles crystallised from lactose alone, all crystallised carrier particles showed higher $R_{elongation}$ than commercial particles confirming their more elongated shape (Fig. 4). As the lactose content of the crystallisation solution was increased, so the elongation of the particles decreased According to ASTM D 2488-00 criteria (28), carrier particles

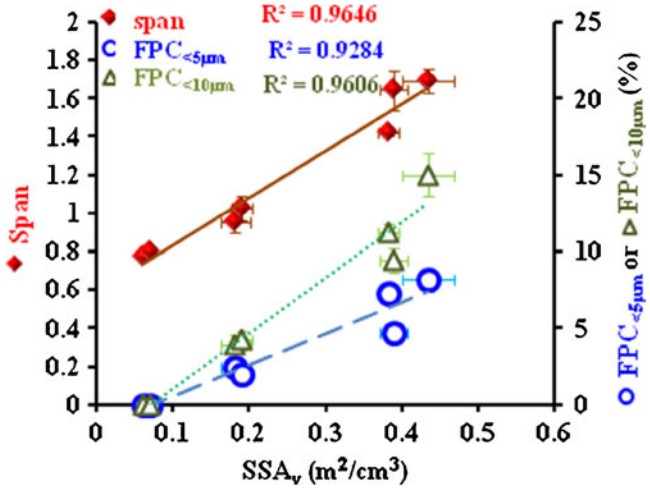


**Fig. 2** Relationships between specific surface area ($SSA_v$), (♦) span, and fine particles [(○) $FPC_{<5\mu m}$, (Δ) $FPC_{<10\mu m}$] for commercial mannitol, commercial lactose, and different crystallised mannitol:lactose (20:0, 15:05, 10:10, 05:15, 0:20) particles (mean ± SE).

crystallised from mannitol:lactose (20:0) and (15:05) could be described as "elongated" ($R_{elongation} > 3$). Crystallised mannitol, crystallised lactose, and crystallised mannitol:lactose samples have markedly different morphologies which could be related to different mechanism of crystal nucleation and crystal growth during crystallisation which is influenced by crystal structure. Acetone has a dehydration influence on α-lactose monohydrate (pesudopolymorphic form) (tomahawk-habit) inducing its transition to anhydrous β-lactose (kite-like habit). However, in case of D-mannitol, acetone (containing hydroxyl group) broke the intra- and inter- hydrogen bonding of solid state mannitol inducing polymorphic form conversion of mannitol (29).

## Scanning Electron Microscope (SEM)

The use of only shape factors alone is not sufficient to represent completely the effect of particle shape as the derived factors depend on particle orientation and contact area with other particles, which also can hinder the accuracy of the technique. Therefore, SEM was employed to obtain three dimensional qualitative assessments of shape and surface (Fig. 4). SEM images showed the typical angular shape with wrinkled (rough) surface morphology reported in previous studies for CM (6) and CL (3) (Fig. 4). The particle sizing data generated by laser diffraction was qualitatively supported by SEM micrographs (Fig. 4), which showed both commercial carriers have relatively clean surfaces while the crystallised carriers appeared contain particles which were covered with fines (Fig. 4). These crystallised carrier particles showed considerably different shape and surface morphologies depending on mannitol:lactose ratio used during preparation. Carrier particles crystallised from mannitol alone have elongated shape whereas carrier particles crystallised from lactose alone have an angular shape with a larger size (Fig. 4). Both morphologies could be observed in carrier particles crystallised from solutions containing mannitol:lactose mixtures depending on mannitol:lactose ratio (Fig. 4). Supporting the PSD data (Fig. 1), SEM images showed that carrier crystals crystallised from mannitol:lactose (05:15) have the smallest size whereas CM particles have the largest size (Fig. 4). Also, supporting span values (Table I), it can be seen that crystallised carrier particles were less homogenous in terms of size and shape compared to commercial particles (Fig. 4). This was the case especially for carrier particles crystallised from mannitol:lactose (15:05) and (10:10) where at least two different populations of particles could be visualised (Fig. 4).

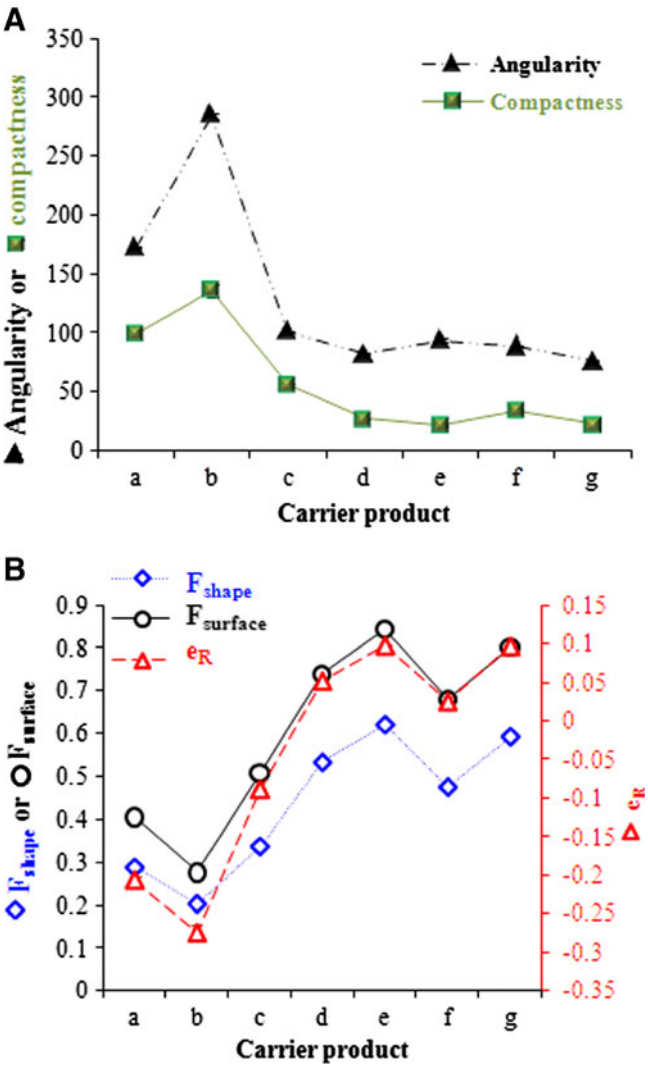


**Fig. 3** (▲) Angularity, (■) compactness, (◊) shape factor ($F_{shape}$), (○) surface factor ($F_{surface}$), and (Δ) simplified shape factor ($e_R$) for commercial mannitol (**a**), commercial lactose (**b**), and different crystallised mannitol:lactose 20:0 (**c**), 15:05 (**d**), 10:10 (**e**), 05:15 (**f**), 0:20 (**g**) particles (mean ± SE, $n \geq 3000$).

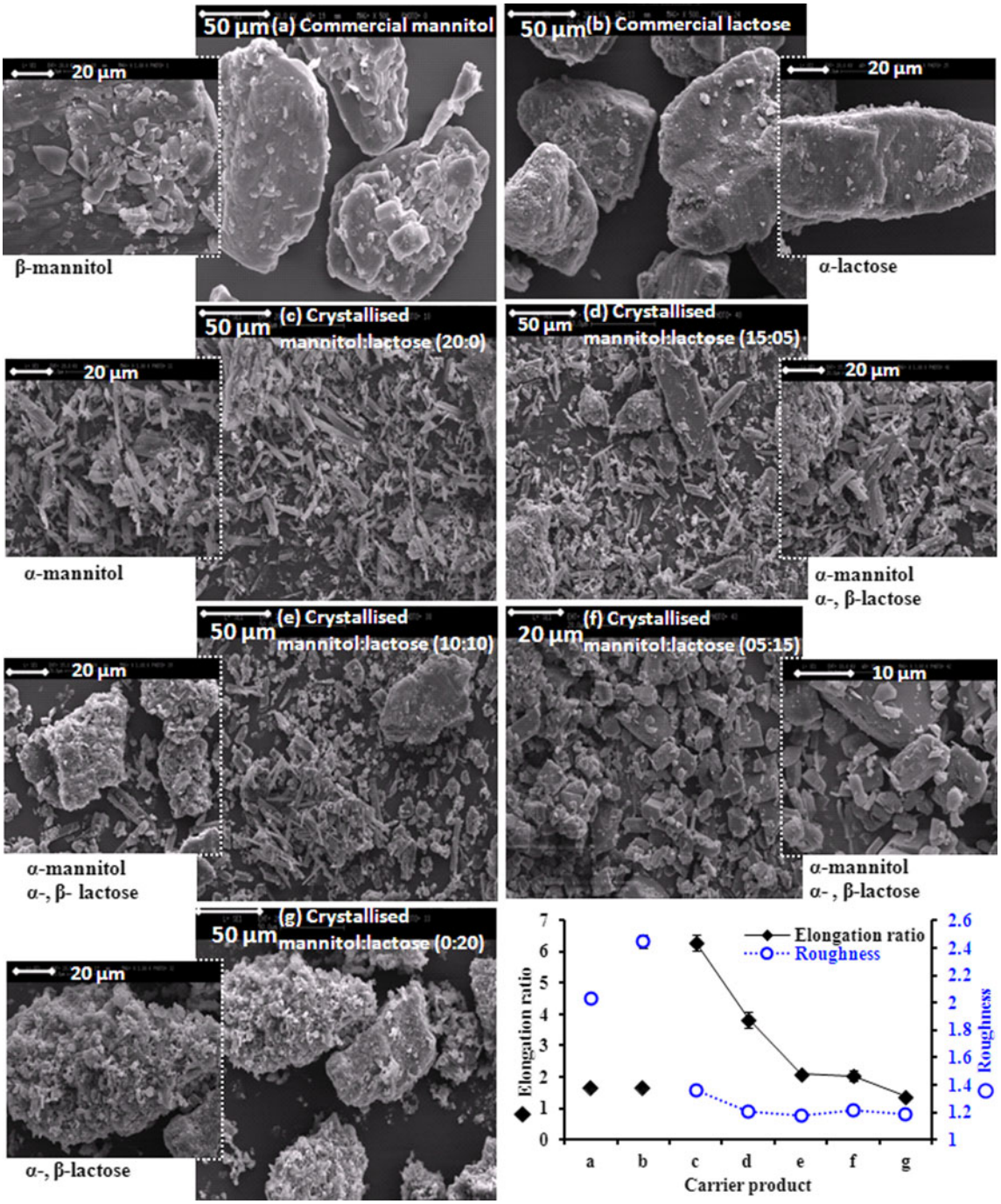


**Fig. 4** SE micrographs, (♦) elongation ratio ($R_{elongation}$), (○) roughness(mean ± SE, $n \geq 3000$) for commercial mannitol (β-mannitol), commercial lactose (α-lactose-monohydrate), and different crystallised mannitol:lactose particles: 20:0 (α-mannitol), 15:05 (α-mannitol + α-, β-lactose), 10:10 (α-mannitol + α-, β-lactose), 05:15 (α-mannitol + α-, β-lactose), and 0:20 (α-, β-lactose).

At unequal ratios of mannitol to lactose [(20:0), (15:05), (05:15)*w*/*w*], the elongated shape of crystallised mannitol tended to dominate (Fig. 4). However, lactose exerted an opposite effect to that of mannitol by reducing the elongation ratio and increasing the width and thickness of the crystals (Fig. 4). At lower ratio of mannitol to lactose (05:15), mannitol restricted the growth of lactose leading to the formation of flat, smooth, thick and the smallest crystals compared to other batches (Table I, Fig. 4). The results from Fig. 1 also showed that particle size distribution of mannitol:lactose (05:15) is skewed towards a smaller size. This could be, in part, arising from the high viscosity of mannitol solution as compared to lactose at the same concentration (30) which is likely to inhibit carrier crystal

growth by restricting the diffusion of solute to the crystal surface.

When an equal ratio of mannitol to lactose (10:10) was present then a balance between the irregular-shaped L (lactose) crystals and the needle-shaped M (mannitol) crystals which could be viewed as co-existing (Fig. 4), suggesting independent crystallisation of the two sugars. Therefore, appropriate size and morphology of carrier crystals can be obtained by judicious addition of mannitol to lactose crystallisation medium.

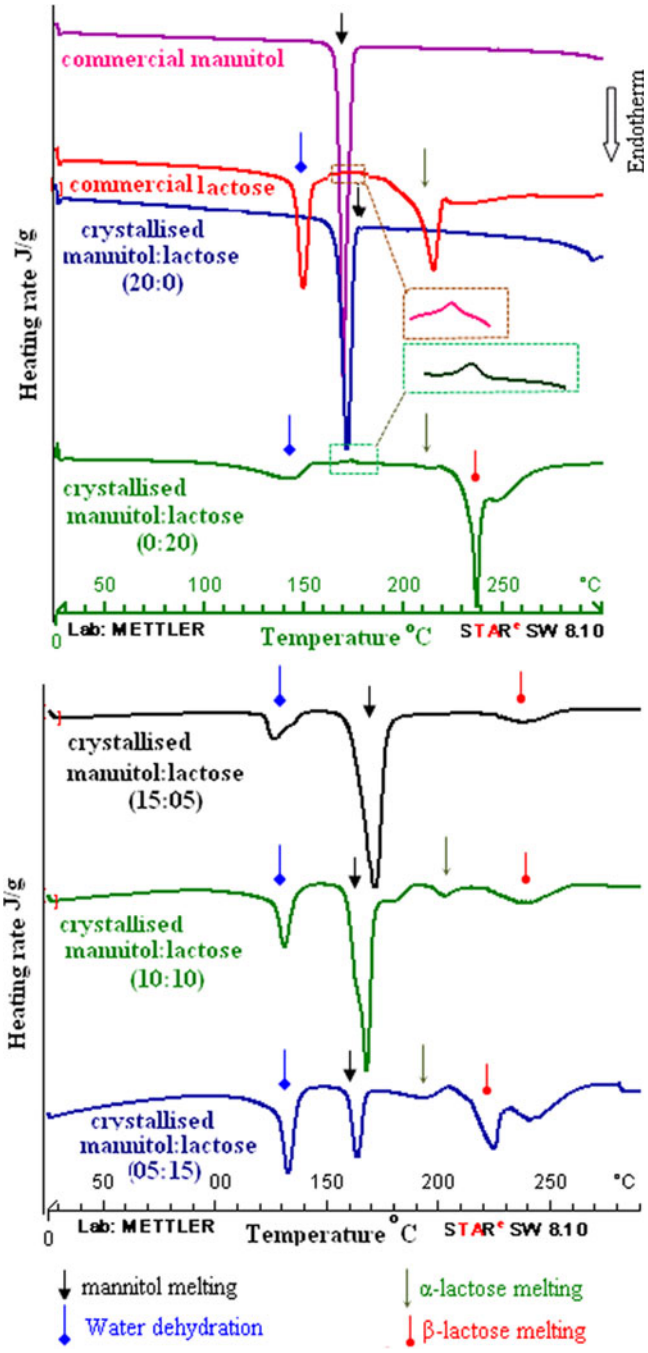


**Fig. 5** DSC thermal traces for commercial mannitol, commercial lactose and different crystallised mannitol:lactose (20:0, 15:05, 10:10, 05:15, 0:20) samples.

## Solid State Characterisation

### *Different Scanning Calorimetry (DSC)*

Thermal transitions inherent in CM, CL, and the different crystallised carrier samples were detected using DSC (Fig. 5). CM and carrier crystallised from mannitol alone showed similar DSC traces containing one endothermic peak at about 167°C corresponding to the melting point of mannitol (7,15). A typical thermal trace for α-lactose-monohydrate was obtained (3,27) when CL was heated, which exhibited two distinctive endothermic events at about 145±5°C and 220±5°C, corresponding to crystalline water dehydration and anhydrous α-lactose melting respectively (Fig. 5). The DSC curve of carrier sample crystallised from lactose alone showed the latter two distinctive endothermic events (with decreased intensities compared to CL) and additional characteristic endothermic event at about 240°C corresponding to the melting point of β-lactose (Fig. 5) (3,27). Carrier particles crystallised from mannitol:lactose (15:05) showed three endothermic events relating to crystalline water dehydration, mannitol melting, and β-lactose melting (Fig. 5). Carrier particles crystallised from mannitol:lactose (10:10) and (05:15) showed four characteristic endothermic events relating to crystalline water dehydration, mannitol melting, anhydrous α-lactose melting, and β-lactose melting (Fig. 5). A small exothermic transition could be observed around 175°C in case of CL and carrier crystallised from lactose alone which is indicative of a small amount of amorphous lactose in these samples (Fig. 5) (3,27). This small transition was not observed in other crystallised carrier samples containing lactose which might be as a consequence of interference with the mannitol melting endothermic peak (Fig. 5). The broad event in the DSC curve after the melting of β-lactose, in case of CL and crystallised carrier from lactose alone and mannitol:lactose (05:15) samples can be ascribed to lactose thermal degradation. Comparison between the enthalpies of different crystallised carrier particles showed that the higher the mannitol concentration the larger the mannitol melting enthalpy (linear, $r^2$=0.9965, figure not shown). Also, the higher the lactose concentration the higher the sum (anhydrous α-lactose+β-lactose) of the melting enthalpies of the two anomers (linear, $r^2$=0.9572, figure not shown). This suggests that the ratio of mannitol:lactose within crystallised carrier product correlated with the ratio introduced within crystallisation media. On the basis of these observations, it is clear that CL particles contain the α-lactose monohydrate whereas carrier particles crystallised from lactose alone contain combination of α-lactose-monohydrate and β-lactose.

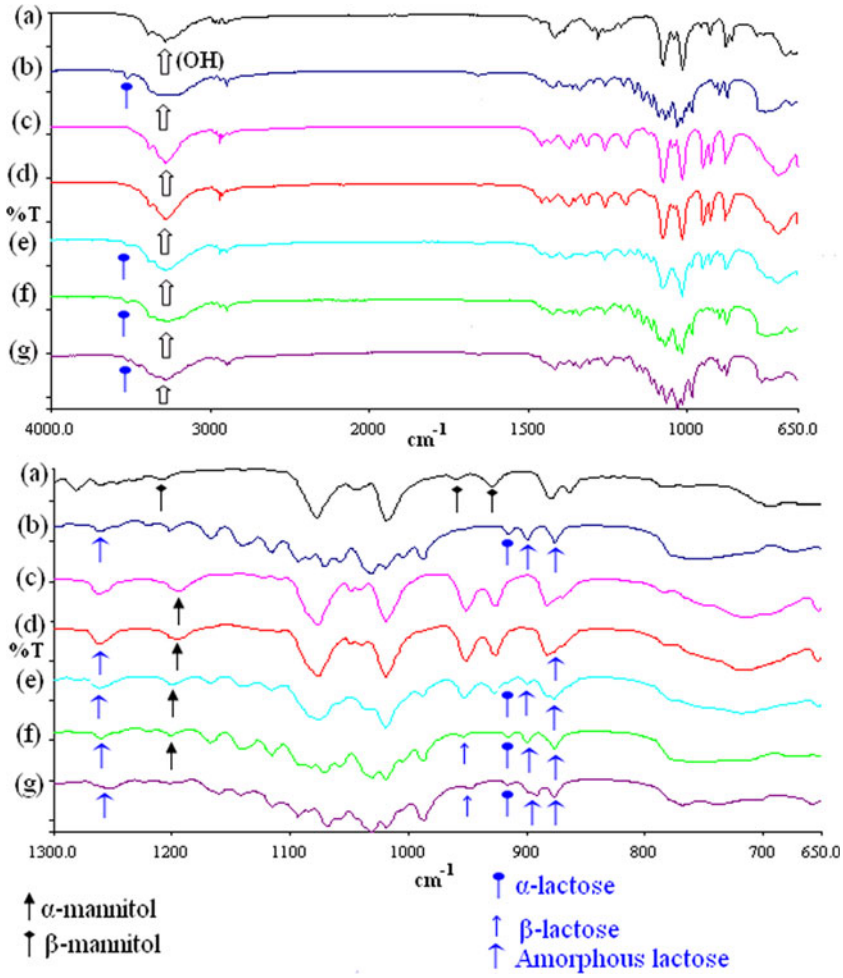


**Fig. 6** FT-IR spectra for commercial mannitol (**a**), commercial lactose (**b**), and different crystallised mannitol: lactose (**c**) 20:0, (**d**)15:05, (**e**) 10:10, (**f**) 05:15, (**g**) 0:20samples.

Crystallised carrier particles from mannitol:lactose (15:05), (10:10), and (05:15) were mixtures of different crystals including α-lactose-monohydrate, β-lactose, and mannitol. In comparison to α-lactose-monohydrate, anhydrous β-lactose is more brittle (31) which might partially account for the higher FPC content in case of samples containing crystallised lactose in comparison to CL (α-lactose-monohydrate).

### *Fourier Transform Infrared (FT-IR)*

FT-IR spectra were used to investigate any changes in crystallized samples in molecular level during the preparation process. FT-IR spectra for CM, CL, and all crystallised carrier particles from 600 to 4000 $cm^{-1}$ and from 600 to 1300 $cm^{-1}$ are shown in Fig. 6. All carrier samples showed a broad band at 3200–3600 $cm^{-1}$ which is related to vibration of the hydroxyl group of mannitol or lactose (32). It has been reported than D-mannitol has at least three common polymorphic forms: α, β and δ (6). Different mannitol polymorphs were shown to have different FT-IR spectra in finger print region of 800–1400 $cm^{-1}$(Table II). Unlike CM and carrier crystallised from mannitol alone; CL and crystallised carrier particles from mannitol:lactose (15:05), (10:10), and (05:15) showed a specific band at 1650 $cm^{-1}$ relating to vibration ofwater hydroxyl groups within the crystals (Fig. 6). Different mannitol or lactose crystal solid state could be characterised according to unique diagnostic peaks as referenced in Table II. Commercial mannitol showed three distinctive peaks at 929 $cm^{-1}$, 959 $cm^{-1}$, and 1209 $cm^{-1}$ which is accounted for by the presence of β-mannitol form (Fig. 6; Table II). Crystallised carrier particles from mannitol:lactose (20:0), (15:05), (10:10), and (05:15) did not show the latter peaks, but showed a peak at 1195 $cm^{-1}$which accounts for the presence of α-mannitol (Fig. 6; Table II). A δ-mannitol specific band (at 967 $cm^{-1}$, Table II) was absent from all carrier products (Fig. 6) suggesting this was absent from all samples.

The bands at 920 $cm^{-1}$ and 3500 $cm^{-1}$ were apparent in CL and carrier samples crystallised from mannitol:lactose (10:10), (05:15), and (0:20) indicating the presence of α-lactose monohydrate (Table II, Fig. 6). The presence of the band at 950 $cm^{-1}$ in carrier particles crystallised from mannitol:lactose (05:15) and (0:20) is likely to be attributable to the existence of β-lactose (Table I, Fig. 6). Absorptions at 875 $cm^{-1}$, 900 $cm^{-1}$, and 1260 $cm^{-1}$, which are indicative

**Table II** Characterisation of Different Mannitol or Lactose Crystal Forms at Various Diffraction Angles (2θ) (XRPD) and Absorption Bands (FT-IR)

| Product | Diffraction angles (XRPD) | References | Band (FT-IR) | References |
|---|---|---|---|---|
| α-mannitol | 9.57°, 13.79° | Kaialy *et al.* (14), Burger *et al.* (35) | 1194 $cm^{-1}$ | Kaialy *et al.* (6, 14), Burger *et al.* (35) |
| β-mannitol | 10.56°, 14.71° | Kaialy *et al.* (14), Burger *et al.* (35) | 1209 $cm^{-1}$, 959 $cm^{-1}$, 929 $cm^{-1}$ | Kaialy *et al.* (6, 14), Burger *et al.* (33) |
| δ-mannitol | 9.74° | Kaialy *et al.* (14), Burger *et al.* (35) | 967 $cm^{-1}$ | Kaialy *et al.* (6), Burger *et al.* (35) |
| α-lactose monohydrate | 12.5°,16.4° | Kaialy *et al.* (15), Haque and Roos (36) | 920 $cm^{-1}$ | Kaialy *et al.* (3, 27, 41), Kirk *et al.* (32) |
| | 12.6° | Traini *et al.* (25) | 3500 $cm^{-1}$ | Kirk *et al.* (32) |
| | 20.0° | Haque and Roos (36), Jouppila *et al.* (37) | | |
| | 20.1° | Jouppila *et al.* (37) | | |
| Anhydrous β-lactose | 10.5°, 20.9°, 21.0° | Haque and Roos (36), Kirk *et al.* (32) | 950 $cm^{-1}$ | Kaialy *et al.* (3, 27, 41), Kirk *et al.* (32) |
| | 10.6° | Traini *et al.* (25) | | |
| α:β lactose (5:3) | 19.1°, 20.1° | Simpson *et al.* (38) | | |
| | 20.0° | Jouppila *et al.* (37), Drapier-Beche *et al.* (39) | | |
| α:β lactose (4:1) | 19.5° | Simpson *et al.* (38), Olano *et al.* (40) | | |
| α-anhydrous | 9.0° | Traini *et al.* (25) | | |

of the presence of amorphous lactose (Table II), were apparent in spectra of CL and carrier crystallised from mannitol: lactose (15:05), (10:10), (05:15), and (0:20) (Fig. 7). From these observations, it can be concluded that CM and CL samples contain β-mannitol and α-lactose monohydrate crystal forms respectively. However, carrier samples crystallised from mannitol or lactose alone contain α-mannitol and α-, β-lactose respectively. Carrier samples crystallised from mannitol:lactose (15:05) showed spectral absorption bands typical of α-mannitol whereas carrier particles crystallised from mannitol: lactose (10:10) showed bands representative of both α-mannitol and α-lactose monohydrate. Carrier particles crystallised from mannitol:lactose (05:15) contain sugars in the form of α-mannitol, α-lactose monohydrate, and β-lactose. Except for CM and carrier samples crystallised from mannitol alone, all carrier samples contain some amorphous lactose.

### *X Ray Powder Diffraction (XRPD)*

Mannitol or lactose crystal form could be distinguished according from XRPD patterns (Fig. 7) as a consequence of the presence of distinctive diagnostic peaks reported in previous studies (Table II). Except for carrier particles crystallised from lactose alone, all crystallised carrier particles showed two diffraction angles at 9.57° and 13.79° which are key characteristic for α-mannitol (Fig. 7; Table II). .All crystallised carrier samples showed two diffraction angles at 12.5° and 16.4° indicating the presence of α-lactose monohydrate (Fig. 7; Table II), except for carrier particles crystallised from mannitol alone. The diffraction angles at 10.5° and 20.9°, which are as characteristic peaks for β-lactose (Table II), were only apparent in carrier samples crystallised from mannitol:lactose (05:15) and (0:20) (Fig. 7). However, based on XRPD patterns at diffraction angles of 19.1° and 19.5° (Table II), crystals with α- and β-lactose in molar ratios of 5:3 and 4:1 (Table II) were formed in case of carrier particles crystallised from mannitol: lactose (15:05), (10:10), (05:15), and (20:05) (Fig. 7). For carrier samples crystallised from higher lactose concentrations, XRPD relative peak intensities for 5α-/3β-lactose (at a diffraction angle of 19.1°) and 4α-/1β-lactose (at a diffraction angle of 19.5°) increased while peak intensities for α-mannitol (at diffraction angle of 9.57°) decreased (Fig. 7). It can be concluded that crystallised lactose (β-lactose anomer) and crystallised mannitol (α-mannitol polymorph) contained different solid state forms compared to their commercial counterpart (α-lactose-monohydrate and β-mannitol polymorph, respectively), as shown from DSC thermograms and confirmed by FT-IR and XRPD patterns (all these forms are known to be kinetically stable). Crystallised mannitol:lactose was shown to contain 5 crystal forms corresponding to α-mannitol, α-lactose-monohydrate, β-lactose, 5α-/3β-lactose and 4α-/1β-lactose (Table III). By analysing the DSC data of M:L (15:05) crystallised carrier, the transition corres-

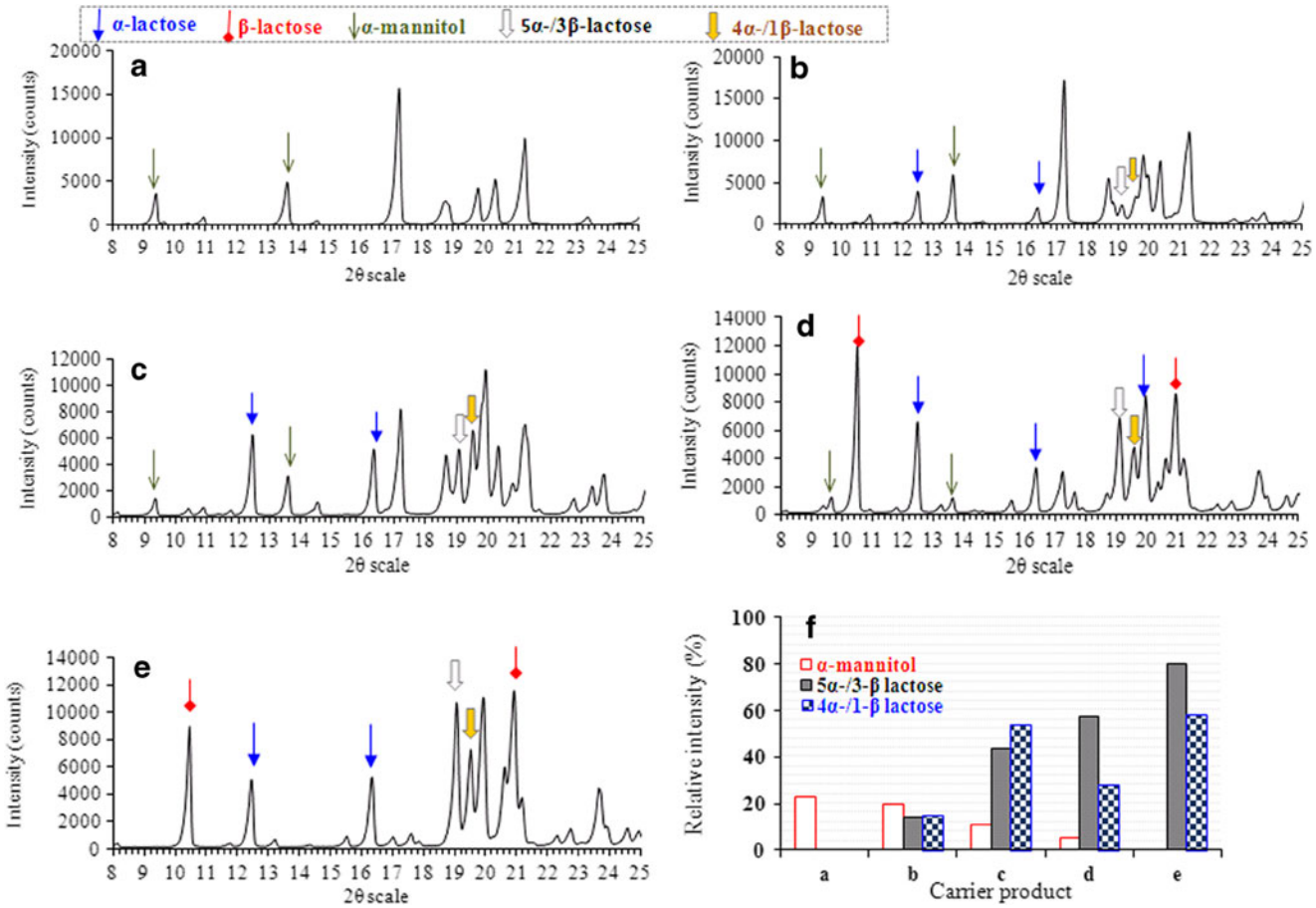


**Fig. 7** XRPD patterns (**a–e**) and relative intensities (**f**) forα-mannitol (at 13.79°), 5α-/3β-lactose (at 19.1°), and 4α-/1β-lactose (at 19.5°) for different crystallised mannitol:lactose 20:0 (**a**), 15:05 (**b**), 10:10 (**c**), 05:15 (**d**), 0:20 (**e**) samples.

ponding to the melting of α/β-lactose was initially thought to correspond to β-lactose, however X-ray powder diffraction spectrum confirmed the existence of 5α-/3β- and 4α-/1β-lactose. Crystallisation of both mannitol and lactose induces change to the solid state forms present in the original sample, as determined from the results derived from the three different analytical techniques. The crystallised carriers also showed some loss in water of dehydration compared to CL (Fig. 7). Solid state transformation of the carrier might not only affect the distribution of any drug adhesion sites upon the surface but also through altering the hardness/brittleness affect the generation of fines (Fig. 4) and hence potentially influence the dispersion and de-aggregation of a drug from DPI formulations.

**Table III** Crystal Form for Commercial Mannitol (CM), Commercial Lactose (CL), and Different Crystallised Mannitol:lactose (M:L) (20:0, 15:05, 10:10, 05:15, 0:20) Products

| | Mannitol | | Lactose | | | | |
|---|---|---|---|---|---|---|---|
| | α | β | α | β | amorphous | α:β (5:3) | α:β (4:1) |
| CM | | ✓ | | | | | |
| CL | | | ✓ | | ✓ | | |
| M:L (20:0) | ✓ | | | | | | |
| M:L (15:05) | ✓ | | ✓ | | ✓ | ✓ | ✓ |
| M:L (10:10) | ✓ | | ✓ | | ✓ | ✓ | ✓ |
| M:L (05:15) | ✓ | | ✓ | ✓ | ✓ | ✓ | ✓ |
| M:L (0:20) | | | ✓ | ✓ | ✓ | ✓ | ✓ |

## Aerosol Performance Assessments

### *Evaluation of SS-Carrier Formulations by SEM*

SEM images of SS, and SS-carrier formulations showed both SS particles (morphologically detected as typical rectangular shape (Fig. 8) (14) and FPC attached to the surface of the large carrier particulate (Fig. 8). This confirms the model of drug-carrier, ordered, interactive mixtures being generated, where small "individual" SS particles adhere to the carrier particles. DPI formulations containing fine carrier particles (e.g. $FPC_{<10\mu m}$ (14)) demonstrate more efficient dispersion than those containing no fine carrier particles. Also, SS particles

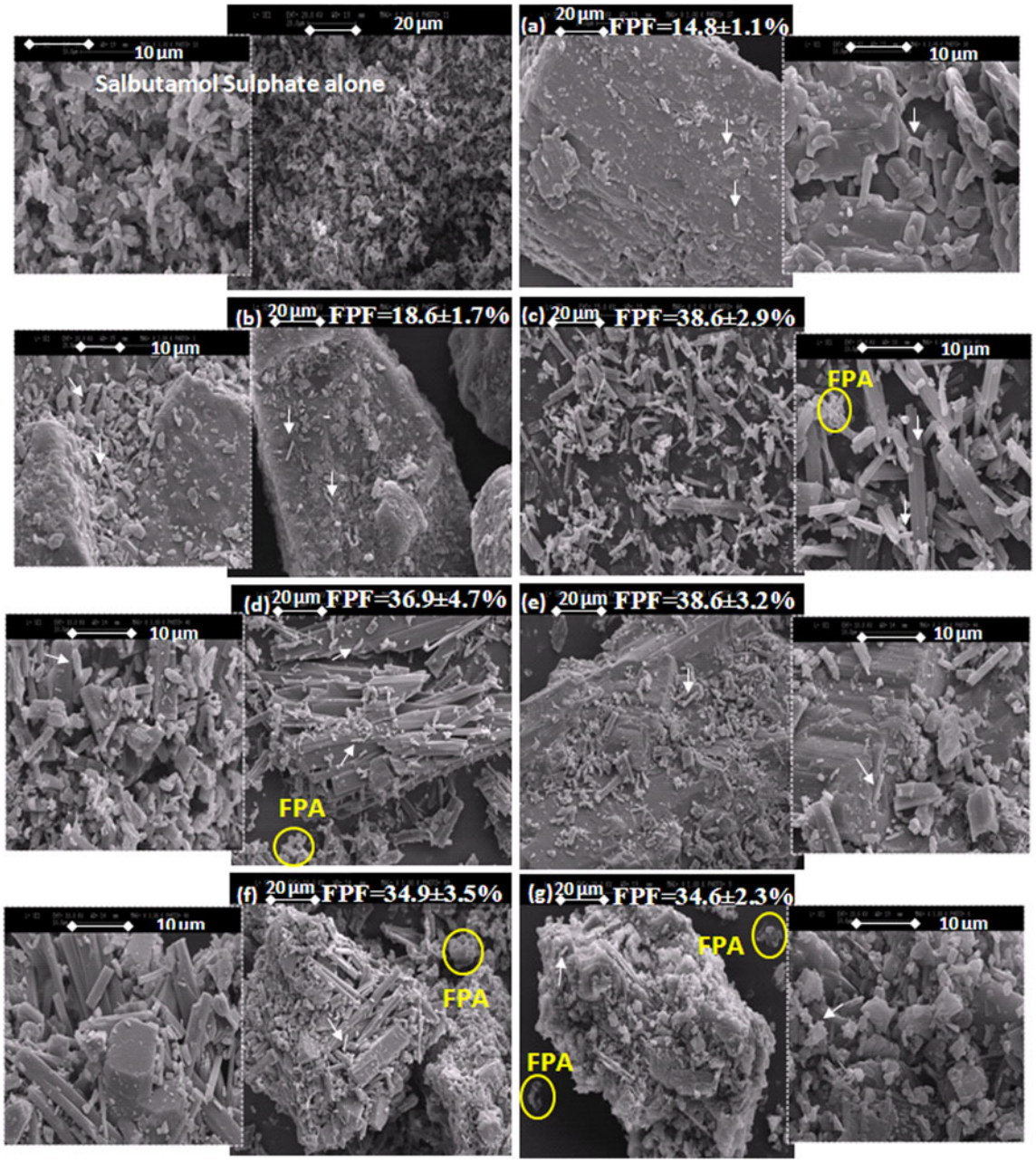


**Fig. 8** SEM of salbutamol sulphate (SS) and for formulations containing SS (indicated by arrows) mixed with commercial mannitol (**a**), commercial lactose (**b**), and different crystallised mannitol:lactose 20:0 (**c**), 15:05 (**d**), 10:10 (**e**), 05:15 (**f**), 0:20 (**g**) samples. (FPA: drug-carrier fine particle aggregate, FPF: fine particle fraction).

can be viewed to carrier particles (Fig. 8) to form fine particle aggregates (FPA: SS + FPC). According to agglomeration theory (16) these FPA are formed at expense of SS-carrier ordered mixtures and might be expected to penetrate to lower airways regions during inhalation.

### *Content Uniformity*

Homogenous drug content is essential to achieve uniform metering doses by the patient during inhalation. Crystallised carriers produced blends with significantly improved drug content homogeneity expressed as % CV (Table IV) in comparison to commercial carriers which did not pass the homogeneity test (CV of 6% is the commonly accepted value as demonstrating satisfactory homogeneity for DPI systems). This might be attributable to the more regular shape of the crystallised carrier particles (Fig. 4) which might lead to better distribution of SS particles on carrier surface during blending and hence reduced variation in SS content within the blend. It is known that blending has a significant effect on DPI performance, especially in case of DPI formulations with low drug mass, due to the effects on

**Table IV** % Uniformity, % Coefficient of Variation (CV), Recovered Dose (RD), Emitted Dose (ED), Fine Particle Fraction ($FPF_{\leq 5\mu m}$), Impaction Loss (IL), Fine Particle Dose ($FPD_{\leq 5\mu m}$), Dispersibility (DS), and Effective Inhalation Index (EI) for Salbutamol Sulphate Obtained from Formulations Containing Commercial Mannitol (CM), Commercial Lactose (CL), and Different Crystallised Mannitol:lactose M:L (20:0, 15:05, 10:10, 05:15, 0:20) Products (mean ± SD, $n=3$)

| | CM | CL | M:L (20:0) | M:L (15:05) | M:L (10:10) | M:L (05:15) | M:L (0:20) |
|---|---|---|---|---|---|---|---|
| Uniformity (%) | 89.9 ± 6.4 | 98.7 ± 10.7 | 92.1 ± 5.3 | 108.5 ± 5.4 | 81.5 ± 4.6 | 91.0 ± 4.2 | 83.2 ± 3.6 |
| CV (%) | 7.1 | 10.9 | 5.8 | 5 | 5.7 | 4.6 | 4.3 |
| RD (μg) | 381.5 ± 8.3 | 317.0 ± 5.1 | 426.6 ± 25.3 | 547.1 ± 33.1 | 454.0 ± 50.8 | 443. 7 ± 70.0 | 395.8 ± 36.7 |
| ED (μg) | 367.3 ± 8.8 | 299.4 ± 6.6 | 396.7 ± 29. 9 | 516. 6 ± 34.9 | 429.9 ± 47.8 | 413.4 ± 83.4 | 374.0 ± 31.9 |
| $FPF_{\leq 5\mu m}$ (%) | 14.8 ± 1.1 | 18.6 ± 1. 7 | 38.6 ± 2.9 | 36.9 ± 4.7 | 38.6 ± 3.2 | 34.9 ± 3.5 | 34.6 ± 2.3 |
| IL (%) | 75.6 ± 0.7 | 67.8 ± 4.7 | 38.0 ± 2.0 | 40.4 ± 6.9 | 39.3 ± 2.7 | 42.3 ± 1.4 | 43.4 ± 3.5 |
| $FPD_{\leq 5\mu m}$ (μg) | 56.7 ± 5.6 | 58.9 ± 4.3 | 165.0 ± 20.0 | 201.9 ± 28.8 | 176.1 ± 30.8 | 156.3 ± 38.3 | 137.1 ± 19.5 |
| DS (%) | 15.4 ± 1.1 | 19.7 ± 1. 9 | 41.5 ± 2.6 | 39.2 ± 4.9 | 40.8 ± 3.2 | 37.6 ± 1.7 | 36.6 ± 2.4 |
| EI (%) | 37.8 ± 1.5 | 41.9 ± 1.8 | 59.9 ± 2.7 | 58.9 ± 3.9 | 60.4 ± 2.6 | 56.9 ± 4.5 | 57.1 ± 1.9 |

interparticulate forces within DPI formulation. Therefore, for the comparison purposes as required here, no further blending optimization was carried out for each type of formulation.

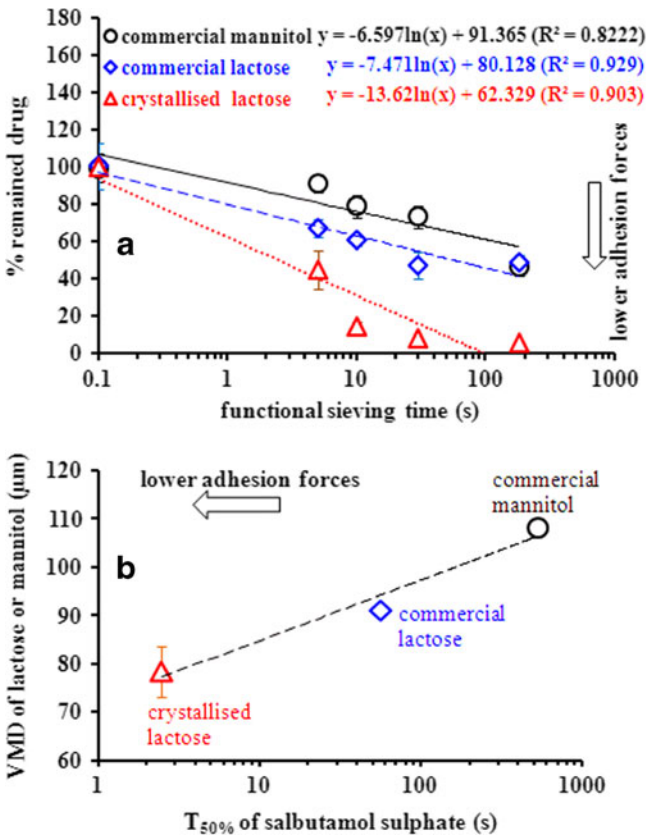


**Fig. 9** % amounts of salbutamol sulphate collected from top of 45 μm sieve after different functional sieving times obtained from formulations containing (○) commercial mannitol, (◊) commercial lactose, or (**Δ**) crystallised lactose (mean ± SD, $n \geq 3$).

### *Evaluation of Drug-Carrier Adhesion Forces*

Upon air jet sieving, small SS particles are expected to detach from large carrier particle surfaces. Fig. 9a shows that for SS-CM, SS-CL, and SS-crystallised lactose formulations, the amounts of SS retained decreased as the sieving time of SS-CM, SS-CL, and SS-crystallised lactose formulations, increased, confirming that these formulations are ordered (Fig. 9a). By plotting amounts of retained SS against sieving time on log scale logarithmic relationships were established (Fig. 9a) from which $T_{50\%}$ was calculated (defined as the time at which 50% of SS particles had detached from carrier particles due to air jet sieving process). $T_{50\%}$ was 528.6 s, 56.4 s, and 2.5 s for formulations containing CM, CL, and crystallised lactose respectively. Such results indicating that SS-carrier adhesion forces were in the following rank order according to carrier type: CM > CL > crystallised lactose.

A plot of $T_{50\%}$ against carrier VMD produced a logarithmic relationship indicating that the larger the carrier particles the higher SS-carrier adhesion (Fig. 9b). Larger carrier particles exhibit higher collision and friction forces during mixing process which might act as press-on forces (adhesive forces). Also, based on Zimon's resuspension model (33), it can be assumed that the larger the carrier particle size, the longer the distance that the drug particles have to slide on carrier surface and thus the greater the drag (or aerodynamic) force. Moreover, decreased drug-carrier adhesion forces in case of crystallised lactose could be attributed to the presence of greater amounts of fine particles and/or the smoother surface (Table I; Fig. 4) of crystallised lactose particles, both of which can lead to a decreased drug-carrier contact area. The SS particles adhered to the surface of CM detached less easily (efficiently) compared to CL from which SS particles detached less efficiently than crystallised lactose.

### *Deposition Study*

Formulations containing crystallised carriers produced considerably different deposition profiles of SS compared to those obtained from those which integrated commercial carriers (Fig. 10). Amounts of SS remained on I&M (or drug loss) ranged between 3.7±0.2% and 7.2±5.4% (Fig. 10A) and could, in part, be ascribed to electrostatic attraction between drug particles and inhaler walls which could not be overcome by the flow rate employed. The amounts of SS deposited on the throat (IP) was considerably higher from formulations containing crystallised carriers (7.9±1.2 – 10.1±1.8%, $P > 0.05$) (Fig. 10A). This might be attributable to the smoother surface and higher amounts of fine particles in case of crystallised carrier products (Table I; Fig. 4). Fine carriers can form agglomerates with SS which deposit in the throat. Also, particles with smoother surface have larger aerodynamic diameter (due smaller drag forces (or surface fractal dimension)) and reduced settling velocity (9,42) and consequently increased probability of impaction. In comparison to commercial carriers, crystallised carriers deposited considerably smaller amounts of SS on MLSI-stage 1, but higher amounts stages 2, 3, 4, and filter (Fig. 10A). These findings indicate that, compared to commercial carriers, SS adhered to crystallised carrier particle surfaces detached more efficiently.

Figure 10B demonstrates that the PSD of SS was dependent on formulation type: SS-CM>SS-CL>SS-crystallised carrier > row SS powder. It is clear the PSD of aerosolised SS (analysed by MSLI) was larger than powdered SS alone (measured by laser diffraction) (Fig. 10B). This could be attributed to particle cohesiveness of SS particle (Fig. 8) and/or the poor dispersing efficiency of inhaler device when operated under these conditions. The aerodynamic PSDs of SS generated from SS-crystallised formulations were smaller than SS-commercial carrier formulations. This indicates that crystallised carriers out-performed CL which in turn outperformed CM in terms of SS aerosolisation efficiency. However, MMAD and GSD of SS obtained from all formulation were similar (3.2±0.2 μm and 2.1±0.0 for MMAD and GSD respectively, $P > 0.05$).

All crystallised carriers produced smaller IL, higher RD, higher ED, higher $FPD_{\leq 5\mu m}$, higher $FPF_{\leq 5\mu m}$, higher DS, and higher EI than commercial carriers (Table IV). This confirms the improved aerosolisation performance for crystallised carrier particles. Both ED and $FPF_{\leq 5\mu m}$ were observed to follow a similar rank order depending on carrier type: crystallised> CL>CM. Higher ED obtained from formulations containing crystallised carriers, comparing to commercial carriers, could be attributed to smaller carrier particle size and higher carrier particle surface area (Fig. 1; Table I). Smaller IL obtained

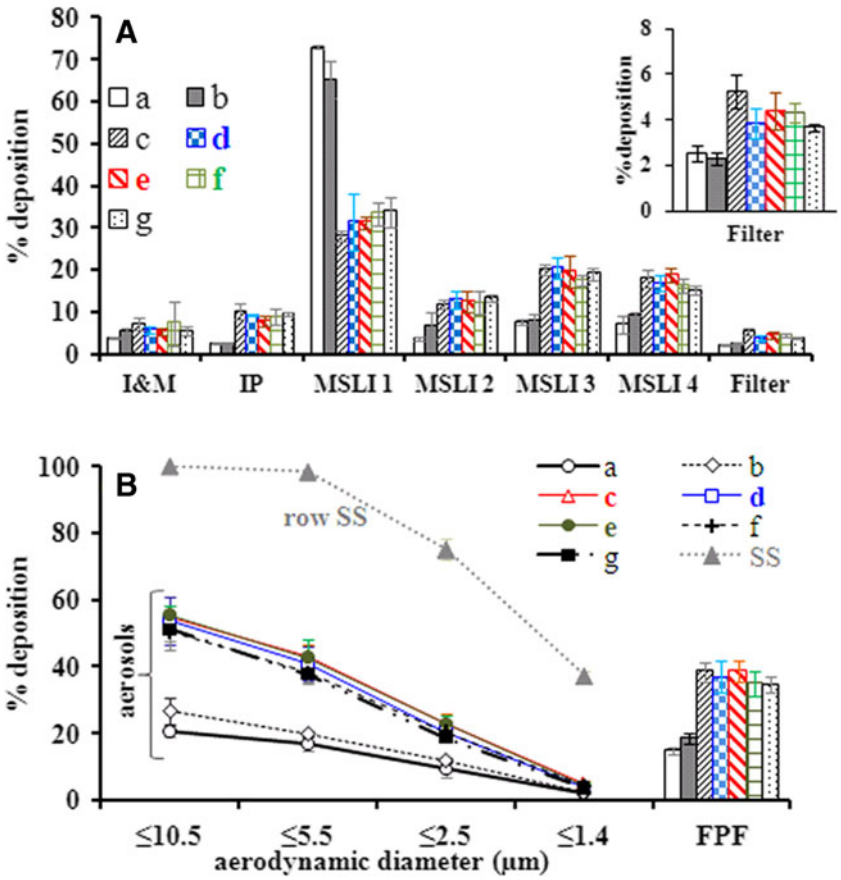


**Fig. 10** MSLI mass distribution of salbutamol sulphate (SS) (**A**), cumulative amounts of SS less than aerodynamic size, and fine particle fraction (FPF) (**B**) obtained from blends containing commercial mannitol (**a**), commercial lactose (**b**), and different crystallised mannitol: lactose (**c**) 20:0, (**d**) 15:05, (**e**) 10:10, (**f**) 05:15, (**g**) 0:20powders (mean ± SD, $n \geq 3$).

from formulations containing crystallised carriers (Table IV) is indicative of smaller amounts of SS particles being adhered to carrier surface (have not been liberated during aerosolisation) compared to commercial carriers. The $FPF_{\leq 5\mu m}$is usually related to drug percentage fraction which is pharmacologically active. Differences in carrier physical properties are believed to be responsible for different SS deposition profiles. Comparing to commercial carriers, higher $FPF_{\leq 5\mu m}$ obtained from blends containing crystallised carriers could be ascribed to increased carrier surface area, higher fines content, and smoother carrier surface as seen in Table I (14,27,34,43). In this study, no simple relationship was observed between carrier particle density ($D_{true}$), size descriptor (e.g. VMD, $SSA_v$, $FPC_{<5\mu m}$, $FPC_{<10\mu m}$, span), or shape descriptor (e.g. angularity, compactness, $F_{shape}$, $F_{surface}$, $e_R$, elongation ratio, or roughness) and FPF of drug. In fact, linear regression analysis of such descriptors gave $R^2$ values less than 0.6 suggesting that there are no readily apparent relationships between the physical properties (density, size, and shape) of carriers investigated in this study and drug *in vitro* aerosolization performance. However, regardless of variations between different crystallised carrier particles, the rank order of $FPF_{\leq 5\mu m}$ of SS (according to carrier type: crystallised>CL>CM) correlated with the specific surface area of the carrier whereas it inversely correlated with VMD, indicating that carrier particles with larger mean diameter and smaller specific surface area produced smaller $FPF_{\leq 5\mu m}$ of SS upon inhalation (Fig. 11a). Such observation may be a consequence of the increased drug-carrier adhesion (Fig. 9) and carrier surface rugosities (Fig. 4) in the case of larger carrier particles. A plot of $FPF_{\leq 5\mu m}$ of SS against amounts of SS retained after 30 s sieving (Fig. 11b) suggested that the lower the SS-carrier adhesion forces the higher the fine particle fraction of SS. Statistical correlation analysis (data not shown) suggested that carrier surface roughness had the largest relative negative impact on FPF whereas the amount of fine carrier particles present had the largest positive impact on FPF.

Finally, it should be noted that crystal form, size, and aerosolisation performance for different carrier products were not significantly affected after being stored for at least 12 months in ambient conditions (22±2°C, 50±2% RH) (data not shown). However further systemic stability studies on the different carrier products at elevated temperatures and humidity may be warranted.

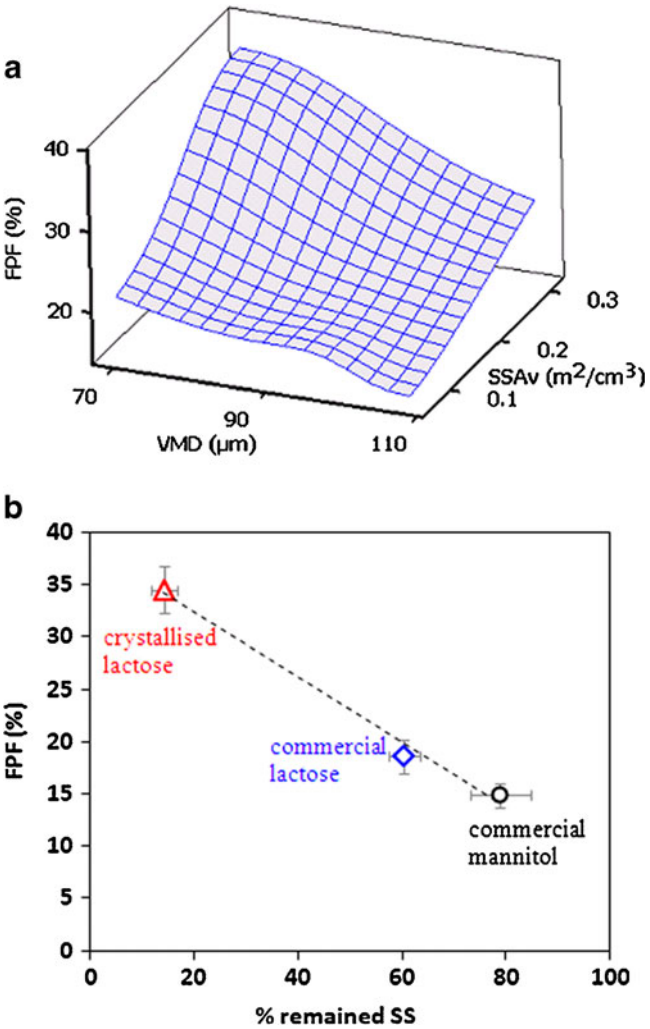


**Fig. 11** Fine particle fraction (FPF) of salbutamol sulphate (SS) in relation to carrier volume mean diameter (VMD), specific surface area ($SSA_v$), and amounts of SS remained after 30 s air jet sieving for DPI formulations containing (○) commercial mannitol, (◊) commercial lactose, and (**Δ**) crystallised mannitol:lactose carriers (mean ± SE, $n \geq 3$).

## CONCLUSION

Mannitol:lactose crystallised carrier particles were prepared in different ratios and characterized in terms of physicochemical properties and *in vitro* DPI performance. All crystallised carrier particles showed more regular shape, higher fines content, and higher specific surface area. Crystallised carrier properties were dependent on mannitol:lactose ratio used during crystallisation. Carriers crystallised using higher mannitol:lactose ratio have a higher elongation ratio, a more irregular shape, and a smaller true density. The change in the solid state forms by the crystallisation process of the carriers may have contributed a side other morphological features to the change in fine particle fraction of salbutamol sulphate. For instance mannitol has changed from spheroidal to needle shape, but also there was a change in its polymorphic form from β-form to α-form, similarly lactose has changed from α-anomer form for commercial lactose to β-anomer form for crystallised lactose. Therefore, formulators can anticipate that appropriate size, solid state, and morphology of lactose carrier can be controlled by judicious addition of mannitol to the crystallisation medium.

Compared to commercial carrier products and regardless of carrier type (mannitol or lactose), all crystallised carrier

powders produced improved drug content homogeneity and higher fraction of drug delivered to lower airway regions upon inhalation indicating their enhanced DPI performance. Carriers with smaller mean diameter, higher specific area, and smaller drug-carrier adhesion properties produced higher fine particle fraction. This research opens up a new window for researchers to investigate the influence of sugar additives (in addition to mannitol) on the physicochemical and aerosolisation performance of lactose to fully understand the effect of carrier particles and determine which factors have the dominating influence on DPI performance.

## ACKNOWLEDGMENTS & DISCLOSURES

Waseem Kaialy thanks Dr Ian Slipper (School of Science, University of Greenwich) for taking SEM images. The authors also thank Roquette for providing mannitol samples.

## REFERENCES

1. Coates MS, Fletcher DF, Chan HK, Raper JA. Effect of design on the performance of a dry powder inhaler using computational fluid dynamics. Part 1: Grid structure and mouthpiece length. J Pharm Sci. 2004;93:2863–76.
2. Hindle M, Jashnani RN, Byron PR. Dose emissions from marketed inhalers: Influence of flow, volume and environment. Respiratory Drug Delivery IV. Interpharm Press Inc., Buffalo Grove, IL, USA. 1994;137–42.
3. Kaialy W, Martin GP, Ticehurst MD, Royall P, Mohammad MA, Murphy J, Nokhodchi A. Characterisation and deposition studies of recrystallised lactose from binary mixtures of ethanol/butanol for improved drug delivery from dry powder inhalers. The AAPS Journal. 2011;13:30–43.
4. Anderson PJ. Delivery options and devices for aerosolized therapeutics. Chest. 2001;120:89S–93S.
5. Esmen NA. Adhesion and aerodynamic resuspension of fibrous particles. J Environ Eng. 1996;122:379–84.
6. Kaialy W, Momin MN, Ticehurst MD, Murphy J, Nokhodchi A. Engineered mannitol as an alternative carrier to enhance deep lung penetration of salbutamol sulphate from dry powder inhaler. Colloid Surface B. 2010;79:345–56.
7. Jones MD, Harris H, Hooton JC, Shur J, King GS, Mathoulin CA, Nicol K, Smith TL, Dawson ML, Ferrie AR, Price R. An investigation into the relationship between carrier-based dry powder inhalation performance and formulation cohesive-adhesive force balances. Eur J Pharm Biopharm. 2008;69:496–507.
8. Ooi J, Traini D, Hoe S, Wong W, Young PM. Does carrier size matter? A fundamental study of drug aerosolisation from carrier based dry powder inhalation systems. Int J Pharm. 2011;413:1–9.
9. Donovan MJ, Smyth HDC. Influence of size and surface roughness of large lactose carrier particles in drypowder inhaler formulations. Int J Pharm. 2010;402:1–9.
10. Dickhoff BHJ, de Boer AH, Lambregts D, Frijlink HW. The effect of carrier surface and bulk properties on drug particle detachment from crystalline lactose carrier particles during inhalation as a function of carrier payload and mixing time. Eur J PharmBiopharm. 2003;56:291–302.
11. Shur J, Harris H, Jones MD, Kaerger JS, Price R. The role of fines in the modification of the fluidization and dispersion mechanism within dry powder inhaler formulations. Pharm Res. 2008;25:1931–40.
12. Donovan MJ, Kim SH, Raman V, Smyth HDC. Dry powder inhaler device influence on carrier particle performance. J Pharm Sci. 2012;101:1097–107.
13. Guenette E, Barrett A, Kraus D, Brody R, Harding L, Magee G. Understanding the effect of lactose particle size on the properties of DPI formulations using experimental design. Int J Pharm. 2009;280:80–8.
14. Kaialy W, Martin GP, Ticehurst MD, Momin MN, Nokhodchi A. The enhanced aerosol performance of salbutamol from dry powders containing engineered mannitol as excipient. Int J Pharm. 2010;392:178–88.
15. Kaialy W, Alhalaweh A, Velaga SP, Nokhodchi A. Effect of carrier particle shape dry powder inhaler performance. Int J Pharm. 2011;421:12–23.
16. Kaialy W, Martin GP, Larhrib H, Ticehurst MD, Kolosionek E, Nokhodchi A. The influence of physical properties and morphology of crystallised lactose on delivery of salbutamol sulphate from dry powder inhalers. Colloid Surface B. 2011;89:29–39.
17. Lucas P, Clarke MJ, Anderson K, Tobyn MJ, Staniforth JN. The role of fine partilce excipients in pharmaceutical dry powder aerosols. Drug Delivery to the Lungs VI. 1998;VI:243–50.
18. Shah KR, Hussain MA, Hubert M, Farag Badawy SI. Form conversion of anhydrous lactose during wet granulation and its effect on compactibility. Int J Pharm. 2008;357:228–34.
19. Dalby RN, Byron PR, Peart J, Suman JD, Farr SJ. Respiratory drug delivery IX. Palm Desert, California: Davis Healthcare International; 2004.
20. Nakate T, Yoshida H, Ohike A, Tokunaga Y, Ibuki R, Kawashima Y. Formulation development of inhalation powders for FK888 with carrier lactose using spinhaler® and its absorption in healthy volunteers. J Controlled Release. 2004;97:19–29.
21. Arnold K, Grass P, Knecht A, Roos R, Sluke G, Thieme H, Wenzel J. Powders for inhalation. US patent. 1995;5478578.
22. Kawashima Y, Serigano T, Hino T, Yamamoto H, Takeuchi H. Effect of surface morphology of carrier lactose on dry powder inhalation property of pranlukast hydrate. Int J Pharm. 1998; 172:179–88.
23. Rabbani NR, Seville PC. The influence of formulation components on the aerosolisation properties of spray-dried powders. J Controlled Release. 2005;110:130–40.
24. Zeng XM, Martin GP, Marriott C, Pritchard J. The use of lactose recrystallised from carbopol gels as a carrier for aerosolised salbutamol sulphate. Eur J Pharm Biopharm. 2001;51:55–62.
25. Traini D, Young PM, Thielmann F, Acharya M. The influence of lactose pseudopolymorphic form on salbutamol Sulfate–Lactose interactions in DPI formulations. Drug Dev Ind Pharm. 2008; 34:992–1001.
26. Young PM, Chan H, Chiou H, Edge S, Tee THS, Traini D. The influence of mechanical processing of dry powder inhaler carriers on drug aerosolization performance. J Pharm Sci. 2007;96:1331–41.
27. Kaialy W, Ticehurst MD, Murphy J, Nokhodchi A. Improved aerosolization performance of salbutamol sulfate formulated with lactose crystallized from binary mixtures of ethanol—acetone. J Pharm Sci. 2011;100:2665–84.
28. ASTM D 2488. Standard practice for description and identification of soils (visual–manual procedure). ASTM west conshohocken. 2000.
29. Yoshinari T, Forbes RT, York P, Kawashima Y. Moisture induced polymorphic transition of mannitol and itsmorphological transformation. Int J Pharm. 2002;247:69–77.
30. Shamil S, Birch GG, Njoroge S. Intrinsic viscosities and other solution properties of sugars and their possible relation to sweetness. Chem Senses. 1988;13:457.

31. Shah SP, Misra A. Liposomal amikacin dry powder inhaler: Effect of fines on *in vitro* performance. AAPS Pharm Sci Tech. 2004;5:107–13.
32. Kirk JH, Dann SE, Blatchford CG. Lactose: a definitive guide to polymorph determination. Int J Pharm. 2007;334:103–14.
33. Zimon AD. Adhesion of dust and powder. New York: Plenum; 1982.
34. Nokhodchi A, Kaialy W, Ticehurst MD. The influence of particle physicochemical properties on delivery of drugs by dry powder inhalers to the lung. In: Popescu MA, editor. Drug delivery book. NY: Hauppauge: Nova; 2011. p. 1–50.
35. Burger A, Henck JO, Hetz S, Rollinger JM, Weissnicht AA, Stöttner H. Energy/temperature diagram and compression behavior of the polymorphs of D-mannitol. J Pharm Sci. 2000;89:457–68.
36. Haque M, Roos Y. Crystallization and X-ray diffraction of spray-dried and freeze-dried amorphous lactose. Carbohydr Res. 2005;340:293–301.
37. Jouppila K, Kansikas J, Roos YH. Crystallization and X–ray diffraction of crystals formed in Water–Plasticized amorphous lactose. Biotechnol Prog. 1998;14:347–50.
38. Simpson TD, Parrish FW, Nelson ML. Crystalline forms of lactose produced in acidic alcoholic media. J Food Sci. 1982;47:1948–51.
39. Drapier-Beche N, Fanni J, Parmentier M. Physical and chemical properties of molecular compounds of lactose. J Dairy Sci. 1999;82:2558–63.
40. Olano A, Bernhard RA, Nickerson TA. Alteration in the ratio of α–to β–lactose co–crystallized from organic solvents. J Food Sci. 1977;42:1066–8.
41. Kaialy W, Ticehurst MD, Nokhodchi A. Dry powder inhalers: Mechanistic evaluation of lactose formulations containingsalbutamol sulphate. Int J Pharm. 2012;423:184–94.
42. Tang HK, Chan JA. Prediction of aerodynamic diameter of particles with rough surfaces. Powder Technol. 2004;146:64–78.
43. Kaialy W, Larhrib H, Nokhodchi A. The effect of carrier particle size on adhesion, content uniformity, and inhalation performance of budesonide using dry powder inhalers. In: Yu-Chaun W, Wei G, editors. Particulate materials: synthesis, characterisation, processing and modelling. Cambridge: Thomas Graham House; 2011. p. 133–9.